Super-Resolution Reconstruction of Electrical Impedance Tomography Images

R. A. Borsoi, J. C. C. Aya, G. H. Costa, *Member, IEEE*, J. C. M. Bermudez, *Senior Member, IEEE*

arXiv:1701.00031v1 [cs.CV] 30 Dec 2016

***Abstract*—Electrical Impedance Tomography (EIT) systems are becoming popular because they present several advantages over competing systems. However, EIT leads to images with very low resolution. Moreover, the nonuniform sampling characteristic of EIT precludes the straightforward application of traditional image ruper-resolution techniques. In this work, we propose a resampling based Super-Resolution method for EIT image quality improvement. Preliminary results show that the proposed technique can lead to substantial improvements in EIT image resolution, making it more competitive with other technologies.**

***Index Terms*—Tomography, Image resolution, Image reconstruction**

I. Introduction

Real-time imaging systems are particularly important in medicine as they provide useful means of monitoring the patient during medical procedures or in intensive care. Intraoperative image guidance, for example, can reduce pedicle screw misplacement in spinal surgeries. However, most intraoperative imaging systems are expensive, offer radiation risks and do not operate in real-time [1]. Likewise, real-time monitoring can avoid lung overdistension and collapse in mechanical lung ventilation, reducing ventilator-associated pneumonia rates [2].

Electrical Impedance Tomography (EIT) is an imaging method that leads to low cost, highly portable, real-time and radiation-free imaging devices. These characteristics make it suitable for bedside diagnosis and intraoperative imaging. However, the lower image quality when compared to other tomography methods still keeps EIT from being widely applied in medical diagnosis and guidance.

The image resolution in tomography methods such as Computed Tomography (CT) and Positron Emission Tomography (PET) has significantly improved with the direct application of Super-Resolution Reconstruction (SRR) techniques. SRR consists basically in the reconstruction of a high resolution (HR) image by extracting non-redundant information from several low resolution (LR) images (usually acquired in the presence of motion) of the same object. SRR was originally a technique intended for overcoming physical limitations of optical imaging sensors. More recently, it has been successfully adapted for other imaging systems such as PET and CT, leading to the improvement of the resulting image quality [3].

Although SRR algorithms developed for optical systems require some adaptations for super-resolving tomographic images originating from PET or CT, the principle of operation of these systems is quite similar to that of optical image acquisition systems. An EIT system, on the other hand, is based on different operation principles. It employs diffuse electrical currents instead of a coherent X-ray beam to generate images, which makes the image acquisition process inherently nonlinear. Besides, the use of traditional finite element (FE) techniques for solving the EIT inverse problem leads to an image represented by a nonuniform grid of conductivity values, as opposed to the uniformly sampled images acquired by sensor grids used in optical systems. These characteristics preclude the direct application of traditional SRR methods to EIT.

Recently, a new SRR method has been developed for the reconstruction of optical images generated by hypothetical nonuniform pixel arrays called Penrose Pixels [4]. Penrose tiling is a method of aperiodic tiling that uses different geometric forms at different orientations to fill a plane [5]. Rhombus Penrose tiling is a specific type of aperiodic tiling that employs only two types of rhombus of equal side length. To allow the representation of the nonuniform pixel grid using matrix-vector notation, it is proposed in [4] that the LR images be upsampled to a regular HR grid as soon as they are acquired. The upsampling operation is dependent on the sensor layout map. The resulting image is called Intermediate HR (IHR) image. After upsampling, image registration and SRR algorithms can be applied on the IHR grid, where the processes of downsampling to and upsampling from the nonuniform grid are incorporated to the reconstruction algorithm by means of an acquisition model. This method has been shown to be capable of achieving larger magnification factors than those obtained using regular pixel arrays, as there are no constraints concerning (sub)pixel displacements between the LR observations because the grid has no translational symmetry. Unfortunately, however, such sensor arrays are currently not being manufactured, and this promising technique remains largely without practical application.

In this paper we propose to employ the resampling strategy used in [4] to deal with the aperiodic tiling characteristic of Penrose pixels to develop an SRR method for super-resolving images generated with arbitrarily irregular tiling such as EIT images, which are composed of non-uniformly spaced pixels forming a finite element mesh (FEM). The EIT data acquisition system is modeled as in an optical SRR problem with nonuniform sampling. Preliminary simulation results show substantial improvements in the reconstruction error and in the perceptual quality of the reconstructed images.

This work has been supported by the the National Council for Scientific and Technological Development (CNPq).

R. A. Borsoi and J. C. M. Bermudez are with the Department of Electrical Engineering, Federal University of Santa Catarina, Florianópolis, Brazil

J. C. C. Aya and G. H. Costa are with the Department of Mechanical Engineering, University of Caxias do Sul, Caxias do Sul, Brazil

II. Resampling-based Super-Resolution for EIT

The EIT image formation process, which is derived from the so-called EIT inverse problem, does not resemble an optical image acquisition system. Each acquired image is derived from the EIT inverse problem, which reconstructs the conductivity inside a given domain based on voltage measurements at its boundary, employing finite element methods in the process [2]. The resulting image consists of a nonuniform mesh (i.e. a finite element mesh - FEM) composed of elements of arbitrary sizes and shapes, each one presenting a constant conductivity value. Moreover, the diffuse nature of the electrical currents injected in the boundary of the domain and the ill-posedness of the inverse problem inflict severe distortions on the resulting image. We will assume these distortions to be appropriately represented by a combination of a space invariant blurring and a nonlinear, spatially variant distortion. Hence, the typical mathematical modeling of the EIT image formation is quite different from the model used in optical SRR algorithms.

In this work we propose to model the EIT image acquisition process using a formulation similar to that used for traditional image systems. By considering each element of the finite element mesh as a pixel of a nonuniform sensor, we propose to employ the Penrose SRR strategy to super resolve the low resolution tomography images. The EIT images are upsampled from the finite element mesh into a uniform grid (IHR) before being processed by a super resolution algorithm. As will be discussed later, the reconstruction method also requires the conjugate downsampling process to be performed. It consists on the transition from the IHR to the LR grid, which is done by assigning to each element of the nonuniform mesh the average value of all the pixels within the corresponding area of the IHR grid. This process is illustrated in Figure 1.

It should be noted that by assigning a position for each pixel in the regular IHR grid (which encloses the whole FEM domain), the value of each IHR pixel can be computed straightforwardly during the upsampling process by determining which element of the FEM circumscribes its position. This is performed using the geometric information about the FEM, which is available with the LR EIT images [2].

We also propose to model the non-linear distortions caused by the inverse problem using a linear filtering approximation (such as the typical optical blurring model), thereby only addressing the space invariant and more well-behaved part of the blurring process. Although the nonlinear and spatially varying portion of the distortion is not accounted for, it shall nevertheless be shown that the resulting SRR performance employing this model is good enough for practical purposes. This new formulation allows the direct application of image SRR techniques to EIT images.

III. The Proposed EIT Imaging Model

The proposed model for the EIT image formation can be mathematically described as

$$\mathbf{y}(t) = \mathbf{H}_{\mathrm{D}}(t)\mathbf{H}_{\mathrm{B}}(t)\mathbf{x}(t)\,, \tag{1}$$

where t is the temporal index, $\mathbf{x}(t)$ is the lexicographically ordered desired uniform HR image, and the vector $\mathbf{y}(t)$, with the same dimension of $\mathbf{x}(t)$, is the lexicographically ordered uniform IHR image. Notice that the EIT LR image is the downsampled IHR image $\mathbf{y}_{\triangle}(t) = \downarrow \mathbf{y}(t)$, where $\downarrow$ represents the downsampling operation illustrated in Figure 1. The resulting LR image, $\mathbf{y}_{\triangle}(t)$, is a mesh composed of nonuniformly distributed elements (pixels), each with constant conductivity.

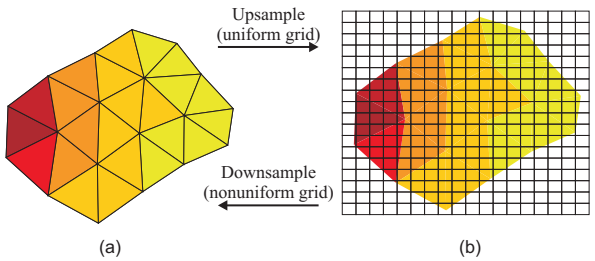

Fig. 1. Illustration of the resampling process. (a) EIT image given by a nonuniform mesh, with constant conductivity value per element. (b) IHR image on the uniform grid. The upsampling process consists of sifting the finite element mesh in order to generate an uniform IHR. The downsample process averages every pixel on the uniform grid that falls within the area of a single element of the mesh, assigning this value for the corresponding element on the nonuniform grid.

The matrix $\mathbf{H}_{\mathrm{B}}(t)$ models the EIT distortion with the linear approximation previously discussed, which can be computed in the form of a convolution operator. Matrix $\mathbf{H}_{\mathrm{D}}(t)$ is a spatially variant kernel convolution matrix performing the transformation from the HR to the IHR grid. Differently from the decimation performed in traditional SRR, $\mathbf{H}_{\mathrm{D}}(t)$ in (1) is a square matrix which is constructed based on the finite element mesh. When processed by this operator, each pixel $y_i(t)$ of the resulting IHR image lying within the area of the p-th nonuniform LR image element $y_{\triangle_p}(t)$ gets assigned the value corresponding to the average of all pixels in the HR image $x_j(t)$ that falls within the area of that specific element of the nonuniform LR image. This process is illustrated in Figure 1, where matrix $\mathbf{H}_{\mathrm{D}}(t)$ corresponds to downsampling the HR image to the LR grid and upsampling the resulting LR image back to the IHR grid, which basically amounts to averaging the pixel values in each LR region.

Since super resolution works by combining information from multiple low resolution images, the relationship between them must also be described. We here adopt the following dynamical model for the evolution of the image sequence:

$$\mathbf{x}(t) = \mathbf{G}(t)\mathbf{x}(t-1) + \mathbf{s}(t), \tag{2}$$

where $\mathbf{x}(t)$ and $\mathbf{x}(t-1)$ are HR images at adjacent time instants, $\mathbf{G}(t)$ is the warp matrix and $\mathbf{s}(t)$ the innovations vector. The warp matrix is a spatial transformation that represents geometric motion like translation or rotation that happens in the image from time $t-1$ to time t. It is constructed based on the motion estimated through image registration, which is here performed on the IHR images [6]. The innovations represent unpredictable changes happening on the video sequence from $\mathbf{x}(t-1)$ to $\mathbf{x}(t)$, i.e., the part of $\mathbf{x}(t)$ that cannot be described as a linear combination of the pixels in $\mathbf{x}(t-1)$, usually due to scene changes like occlusions.

Since the imaging model proposed for the EIT system given in (1) and (2) is now in the standard form encountered for

traditional optical systems, any traditional SRR algorithm can be applied using the upsampled EIT images as input.

IV. Results

In this section we present preliminary results illustrating the super resolution of EIT images using the imaging model proposed in Section III. Three examples were devised to illustrate the application of the proposed method. The first example presents the reconstruction of images of a T-shaped object subject to translational displacements considering a rough FEM and noisy measurements. The algorithm was tested both with motion known *a priori* and with motion estimated by a registration algorithm. The second example extends the first one to EIT images formed by ellipsoids of varying volume, which emulates the imaging of a breathing thorax. The motion was estimated with a registration algorithm. Finally, a third example presents the super-resolution of EIT images of a breathing thorax obtained from real voltage measurements.

We have applied the Least Mean Squares SRR [7] algorithm to super resolve the images in all the examples, with step size $\mu = 0.01$ and $K = 100$ iterations for each input image. The motion estimation was performed using the *Horn & Schunk* Optical Flow algorithm of [6][1] using IHR image pairs as input. Since the image sequences of Examples 1 and 2 were synthetically generated, the desired HR images were available, allowing a quantitative assessment through the squared error $\|\hat{\mathbf{x}}(t) - \mathbf{x}(t)\|^2_{\mathcal{D}}$ averaged over all image pixels in the region inside the nonuniform mesh domain $\mathcal{D}$.

In all examples, matrix $\mathbf{H}_{\mathrm{D}}(t)$ corresponded to the space-variant kernel associated with the nonuniform mesh of each LR EIT image, which was assumed to be time-invariant. The distortion matrix $\mathbf{H}_{\mathrm{B}}(t)$ was modeled as a space- and time-invariant 60×60 Gaussian convolution mask with standard deviation $\sigma = 20$ and Neumann (symmetric) boundary conditions. The nonuniform LR EIT images were upsampled to a 200×200 IHR uniform grid before processing, where the region outside the nonuniform mesh domain $\mathcal{D}$ was padded with zeros. The EIT inverse problem was solved with EIDORS [8], using the Gauss-Newton solver with the NOSER image prior [9]. The FEM and the solver used in the computation of the EIT inverse problem were selected by focusing on simple solutions with low computational cost to emulate the results that would typically be obtained in real time processing situations. This, however, does not incur any loss of generality for the proposed technique, since the improvements obtained with the SRR algorithm are maintained regardless of the FEM and inverse solver employed.

A. Example 1

In this example, a sequence of 20 images of a T-shaped object subject to random translational motion inside a circular body was generated. The amplitude of the motion was determined by samples of a zero-mean white Gaussian variate with variance 0.3, truncated so that the resulting position was limited to the interval $[-0.15, 0.15]$ to assure that the object lied entirely inside the body.

[1]With parameters `lambda=10`^{6}, `pyramid_levels=4`, `pyramid_spacing=2`.

The EIT images were generated using meshes "d2d1c" and "a2d3c" with 32 electrodes for the direct and inverse problems, respectively. Random noise was added to the voltage measurements of the EIT direct problem, resulting in a signal to noise ratio (SNR) of -5dB. Figure 2(a) shows the synthetic desired image (20-th frame), where the object of interest is clearly identifiable. Figure 2(b) shows the corresponding observation (LR image $\mathbf{y}_{\triangle}(t)$). The reconstruction was performed twice, first considering the motion to be known *a priori* and afterwards estimating it using the registration algorithm in [6].

Figures 2(c) and 2(d) show the reconstruction result for the last (20-th) frame (considering estimated motion) and the evolution of the average squared error for the observed (LR) and reconstructed images. It can be verified that the object of interest in the reconstructed image is more well defined and significantly closer to the original EIT image than the corresponding object in the LR observed EIT image. The average squared error of the reconstructed image considering known motion converged to a value reasonably smaller than that of the observed LR images. Furthermore, a slight degradation in performance was noted when a registration algorithm was employed, leading the average squared error of some frames to be close to or worse than that of the observed LR images. Besides the influence of imprecise motion information, the cost function of the SRR algorithm employed (LMS-SRR) minimizes the error in the mean-square sense, which does not guarantee optimality for any specific sequence/realization. Nevertheless, the improvement in resolution is clearly significant, indicating that the proposed approach is effective in practical scenarios.

B. Example 2

In this example, we performed the reconstruction of a sequence of 20 images of a synthetic lung phantom. A thorax was emulated by a circular body, with ellipses of varying area acting as the lungs, and an additional static circle denoting the spine. Like in Example 1, the EIT images were generated using meshes "d2d1c" and "a2d3c" with 32 electrodes for the direct and inverse problems, respectively. The signal to noise ratio (SNR) of the measurements was chosen to be -5dB. Figure 3(a) shows the synthetic phantom (20-th frame), where the lungs and the spine are visible. Figure 3(b) shows the corresponding observation (LR image $\mathbf{y}_{\triangle}(t)$). The motion between the frames was estimated using the registration algorithm in [6].

Figures 3(c) and 3(d) show the reconstruction result for the last (20-th) frame and the evolution of the mean-square error (MSE) for the observed (LR) and reconstructed images. It can be verified that both the lungs and the spine are clearly visible in the reconstructed image, despite being severely distorted in the corresponding LR observation. The MSE of the reconstructed image converged to a value significantly smaller than that of the observed LR images, corroborating with the perceptual results.

C. Example 3

In this example the proposed technique is employed in super-resolving a sequence of 34 EIT images of a breathing

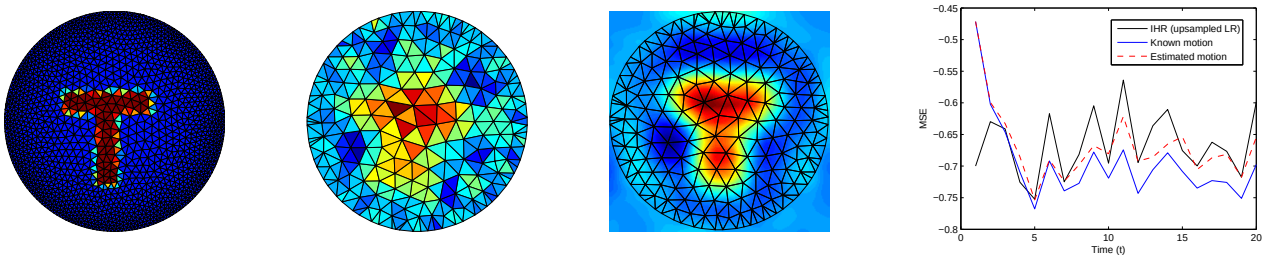

(a) (b) (c) (d)

Fig. 2. Example 1: (a) Synthetic HR image (used in the EIT direct problem). (b) EIT low resolution image. (c) Super-resolved EIT image (the nonuniform mesh was displayed for ease of comparison). (d) Average squared error evolution.

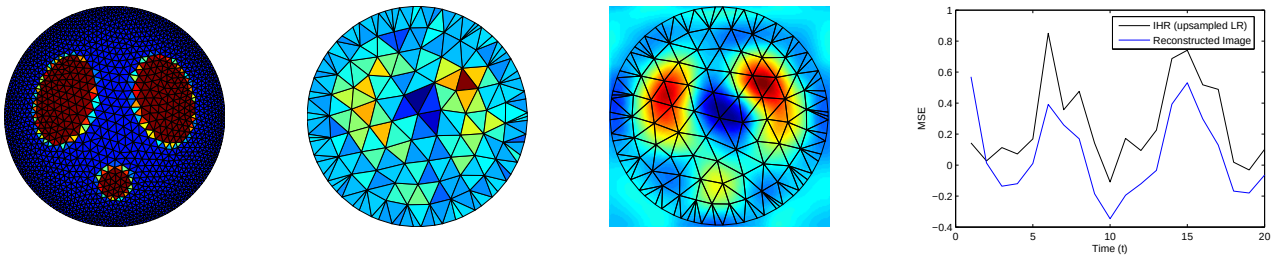

(a) (b) (c) (d)

Fig. 3. Example 2: (a) Synthetic HR image (used in the EIT direct problem). (b) EIT low resolution image. (c) Super-resolved EIT image (the nonuniform mesh was displayed for ease of comparison). (d) Average squared error evolution.

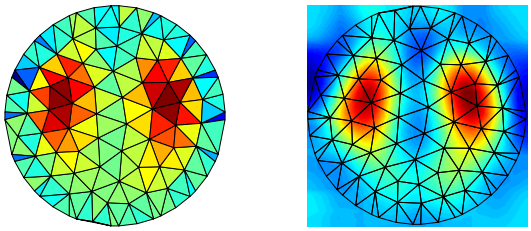

(a) (b)

Fig. 4. Example 3: (a) EIT low resolution image. (b) Reconstructed EIT image (the nonuniform mesh was displayed for ease of comparison).

thorax reconstructed from real data obtained from the *Montreal* Data set [8]. The inverse problem was solved using mesh "a2d1c" with 16 electrodes. The motion between the frames was estimated using the registration algorithm in [6]. Since the HR (desired) images were not available, the MSE could not be evaluated for this example.

Figure 4(a) shows the LR observation (EIT image $\mathbf{y}_{\triangle}(t)$) for the middle (17-th) frame. Figure 4(b) shows the corresponding reconstruction result. This frame was selected because it depicts the middle of the breathing cycle, since images of the filled lungs provide a better visualization of the results. A sensible improvement can be noticed in the reconstructed image, where the lungs are more well defined and more easily identifiable from the image background.

V. Conclusion

In this paper we have proposed a new method for super-resolution reconstruction of EIT images. The proposed method uses a new model for the EIT image formation system, which is based on the Penrose Pixels approach developed for optical image acquisition systems. Although the Penrose Pixels Super-Resolution methodology still has no practical application due to the lack of appropriate sensor, we have shown that its essence can be used to handle the non-conventional imaging sensors typical of EIT images. Simulation results employing the LMS-SRR algorithm show that a significant increase on the visual quality and resolution of EIT images can be achieved with the proposed method, indicating the possibility of mitigating the severe deficiency in image quality that currently prevents EIT imaging systems to be more widely used. The visual quality of the resulting image was significantly improved, and the mean square error between the reconstructed and the HR image decreased substantially when compared to that of the LR observations, indicating that super-resolution effectively has been obtained. Significant improvements were verified for both idealized and practical scenarios.

References

[1] Patrick Helm, Robert Teichman, Steven Hartmann, and David Simon. Spinal navigation and imaging: History, trends, and future. *Medical Imaging, IEEE Transactions on*, 34(8):1738–1746, 2015.

[2] David S Holder. *Electrical impedance tomography: methods, history and applications*. CRC Press, 2004.

[3] John Kennedy, Ora Israel, Alex Frenkel, Rachel Bar-Shalom, Haim Azhari, et al. Super-resolution in PET imaging. *Medical Imaging, IEEE Transactions on*, 25(2):137–147, 2006.

[4] Moshe Ben-Ezra, Zhouchen Lin, Bennett Wilburn, and Wei Zhang. Penrose pixels for super-resolution. *Pattern Analysis and Machine Intelligence, IEEE Transactions on*, 33(7):1370–1383, 2011.

[5] R. Penrose. The role of aesthetics in pure and applied mathematical research. *Bull. Inst. of Math. and its Appl.*, 10:266–271, 1974.

[6] Deqing Sun, Stefan Roth, and Michael J Black. Secrets of optical flow estimation and their principles. In *Computer Vision and Pattern Recognition (CVPR), 2010 IEEE Conf. on*, pages 2432–2439. IEEE, 2010.

[7] Michael Elad and Arie Feuer. Superresolution restoration of an image sequence: adaptive filtering approach. *Image Processing, IEEE Transactions on*, 8(3):387–395, 1999.

[8] Andy Adler and William RB Lionheart. Uses and abuses of EIDORS: an extensible software base for EIT. *Physiol. Meas.*, 27(5):S25, 2006.

[9] Margaret Cheney, David Isaacson, Jonathan C Newell, S Simske, and J Goble. NOSER: An algorithm for solving the inverse conductivity problem. *Int. J. Imag. Syst. Tech.*, 2(2):66–75, 1990.